ACS APPLIED MATERIALS & INTERFACES

Research Article

www.acsami.org

Robust ICG Theranostic Nanoparticles for Folate Targeted Cancer Imaging and Highly Effective Photothermal Therapy

Mingbin Zheng,[†,‡,§] Pengfei Zhao,[‡,§] Zhenyu Luo,[‡,§] Ping Gong,[‡] Cuifang Zheng,[‡] Pengfei Zhang,[‡] Caixia Yue,[‡] Duyang Gao,[‡] Yifan Ma,[‡] and Lintao Cai*[,‡]

[†]Department of Chemistry, Guangdong Medical College, Dongguan 523808, People's Republic of China

[‡]Guangdong Key Laboratory of Nanomedicine, Shenzhen Key Laboratory of Cancer Nanotechnology, Institute of Biomedicine and Biotechnology, Shenzhen Institutes of Advanced Technology, Chinese Academy of Sciences Shenzhen 518055, People's Republic of China

ABSTRACT: Folic acid (FA)-targeted indocyanine green (ICG)-loaded nanoparticles (NPs) (FA-INPs) were developed to a near-infrared (NIR) fluorescence theranostic nanoprobe for targeted imaging and photothermal therapy of cancer. The FA-INPs with good monodispersity exhibited excellent size and fluorescence stability, preferable temperature response under laser irradiation, and specific molecular targeting to MCF-7 cells with FA receptor overexpression, compared to free ICG. The FA-INPs enabled NIR fluorescence imaging to *in situ* monitor the tumor accumulation of the ICG. The cell survival rate assays *in vitro* and photothermal therapy treatments *in vivo* indicated that FA-INPs could efficiently targeted and suppressed MCF-7 cells and xenograft tumors. Hence, the FA-INPs are notable theranostic NPs for imaging-guided cancer therapy in clinical application.

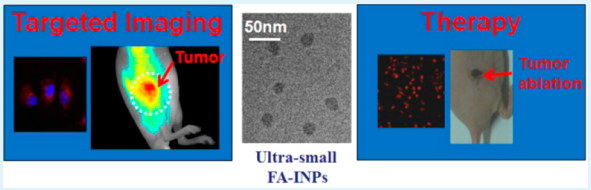

KEYWORDS: *indocyanine green, theranostic nanoparticles, cancer imaging, photothermal therapy, folic acid*

1. INTRODUCTION

Cancer is currently one of the most lethal disease concerns in global healthcare.[1−4] The informative and accurate visualization of anti-cancer agents, following their administration, can play a considerable and indispensable role to formulate effective anti-cancer therapeutics.[5,6] Conventional diagnostic and small molecular therapeutic agents are often limited by nonspecific biodistribution and short blood circulation times.[5] Many efforts have been performed in the areas of multifunctional theranostic nanoparticles (NPs), which integrated targeting, therapeutic, and diagnostic functions together, provide many potential advantages, such as extension of circulating half-life of conventional agents, specific targeting of cancer, monitor the therapeutic efficacy and prognosis in real time.[5−8] A series of nanomaterials have been successfully developed for cancer imaging and therapy including polymeric NPs, quantum-dot, graphene, gold, and magnetic nanomaterials.[9−12] For example, gold nanocages were served as contrast agents for photoacoustic and multimodal (photoacoustic/fluorescence) imaging, and used as photothermal agents for selective destruction of cancerous or diseased tissue.[13] Santra et al. reported taxol/Cy5.5-loaded iron oxide NPs for combined folic acid (FA)-targeted cancer therapy and dual optical/magnetic resonance imaging.[14] Nie et al. designed cyclic Arg-Gly-Asp peptides conjugated plasmonic gold nanostars (RGD-GNS) that clearly imaged tumor angiogenesis with enhanced contrast, and could effectively inhibit tumor growth by photothermal therapy.[15] Indocyanine green (ICG) is approved by the U.S. Federal Drug Administration (FDA) for near-infrared (NIR) clinical imaging agents.[16,17] It is also proved to an effective photosensitive agent by laser-excitation heat for photothermal therapy, generation reactive oxygen species for photodynamic therapy, and strongly ultrasound response for sonodynamic therapy.[16−20] However, application of the free ICG is limited by its numerous defects, including poor aqueous stability, its concentration-dependent aggregation, rapid elimination from the body.[18,21,22]

To overcome these limitations of the free ICG, we directly self-assembled a biodegradable FA-targeted ultrasmall NPs encapsulated ICG (FA-INPs) with intrinsic FA targeted ligands, using the film hydration via strong sonication followed by extrusion technique. The FA-INPs were characterized by dynamic laser scattering (DLS) and transmission electron microscopy (TEM). The size stability, fluorescence properties, and temperature response under laser irradiation were evaluated. Cell-specific targeting and photothermal toxicity of the FA-INPs were investigated in the MCF-7 cells. We further demonstrated the NIR imaging and photothermal therapy of the FA-INPs on the tumor xenograft model. The FA-INPs showed stable NIR fluorescence signals of ICG and targeting recognition of FA receptor over-expressing MCF-7 cells. The FA-INPs were performed as great theranostic NPs for tumor targeted imaging and photothermal therapy.

2. EXPERIMENTAL SECTION

2.1. Materials. ICG, cholesterol, hematoxylin, eosin, and 3-(4, 5-dimethylthiazol-2-yl)-2,5-diphenyltetrazolium bromide

Received: January 21, 2014
Accepted: April 3, 2014
Published: April 3, 2014

   dx.doi.org/10.1021/am5004393 | ACS Appl. Mater. Interfaces 2014, 6, 6709−6716

(MTT) were obtained from Sigma–Aldrich (USA). 1,2-Distearoyl-*sn*-glycero-3-phosphoethanolamine-*N*-folate (poly(ethylene glycol) 2000 (DSPE-PEG-FA) and soybean lecithin were purchased from Avanti (USA). Propidium iodide (PI) and calcein-AM were obtained from Invitrogen (USA). Penicillin–streptomycin, RMPI 1640 without FA, and fetal bovine serum were obtained from Gibco Life Technologies (USA).

2.2. Formulation of the FA-INPs. The FA-INPs were prepared using the film hydration via strong sonication followed by an extrusion technique. Lecithin, cholesterol, ICG, and DSPE-PEG-FA with a mass ratio of 1.7:2:1:1.7 were placed in a round-bottom flask and dissolved in a methanol/chloroform mixture. The organic solvent was removed with a rotavapor to generate a thin film on the glass vial. The film was then hydrated with ultrapure water via 5 min strong sonication with a VCX130 ultrasonics processor (USA). Following hydration, the FA-INPs were obtained by extrusion through 200- and 100-nm polycarbonate filters (five times each).[23−25] Finally, the FA-INPs were washed three times by ultrafiltration (Millipore, Amicon, USA).

2.3. Characterization of the FA-INPs. A Zetasizer Nano ZS (Malvern, U.K.) was used to detect the size of the NPs. The morphologic and particle size of NPs were obtained using TEM (FEI Tecnai G2 F20 S-Twin, USA). The absorption spectra or fluorescence spectra were performed using UV/vis spectrometry (Lambda25, Perkin–Elmer, USA) or fluorescence spectroscopy (F900, Edinburgh Instruments, Ltd., U.K.; ex: 740 nm). ICG concentration of free ICG or the FA-INPs was identified by testing the fluorescent intensity at 810 nm. The ICG concentration was adjusted to 0.01 mg/mL. The quantum yield of the FA-INPs compared to the free ICG was studied. Fluorescence quantum yield (Φ_F) is defined as the ratio of the number of excited-state fluorophores that relax via a fluorescent transition over the number of excited dyes.[26] The Φ_F of the FA-INPs or free ICG in aqueous solution is determined by comparison with a standard (freshly prepared ICG solution in dimethyl sulfoxide, $\Phi_{F\ ref}$ = 13.0%).[26] The Φ_F was calculated using the following equation: $\Phi_F = \Phi_{F\ ref} \times (\eta^2/\eta^2_{ref}) \times (I/A) \times (A_{ref}/I_{ref})$, where $\Phi_{F\ ref}$ is the quantum yield of the reference compound, η is the refractive index of the solvent, I is the integrated fluorescence intensity and A is the absorbance at the excitation wavelength.[26] The encapsulation efficiency (EE) of ICG loaded in NPs was determined as the reported literature.[19]

2.4. Tumor Cells. MCF-7 human breast adenocarcinoma cells, which are of FA overexpression were used for the cell studies. RMPI 1640 medium without FA was supplemented with 1% penicillin, 1% streptomycin, and 10% heat-inactivated fetal bovine serum. Cells were cultivated in humidified environment of 5% CO_2 and in medium at 37 °C.

2.5. *in Vitro* Cellular Uptake. Eight-well chambered coverglasses (Lab-Tek, Nunc, USA) were seeded MCF-7 cells (2×10^4 cells/well, 200 μL of medium). The old medium at 24 h was changed by the medium with free ICG (5 μg/mL of ICG), FA-INPs (5 μg/mL of ICG) or FA-INPs + free FA (5 μg/mL of ICG + 200 μg/mL of FA). After 2 h, PBS washed the cells thrice and 4% paraformaldehyde solution fixed the cells for 20 min, then Hoechst 33258 stained for 10 min and PBS rinsed thrice, finally Leica TCS SP5 confocal laser scanning microscope (GER) was used to observe cellular uptake.

Cell uptake was further quantitatively analyzed with NIR imaging and flow cytometer. MCF-7 cells were seeded in 24-well plate (4×10^5 cells/well) and cultured overnight. Cells were replaced by the medium containing free ICG (5 μg/mL of ICG), FA-INPs (5 μg/mL of ICG) or FA-INPs + free FA (5 μg/mL of ICG + 200 μg/mL of FA). After 2 h, PBS washed the cells thrice and the CRi maestro ex *in vivo* imaging system (USA) was used to collect the fluorescence signals of ICG (704 nm excitation and 735 nm filter). Then the cells were harvested to record the fluorescence histograms of ICG with flow cytometer (BD Accuri C6, USA).

2.6. *in Vitro* Photothermal Toxicity of the FA-INPs. A 96-well plate was seeded with MCF-7 cells (1×10^4 cells/well, 100 μL of medium with free ICG, FA-INPs, or FA-INPs + FA). After 24 h, PBS washed the cells and fresh medium were replaced. Then, the plate was placed on the digital dry bath incubator (Labnet Accublock, USA) to keep 37 °C. The cells were irradiated with/without a 1.6 W/cm^2 808-nm laser for 5 min. MTT assay quantified the cell viability. To directly observe the photothermal therapeutic efficacy, the cells irradiated with laser were washed with PBS and fixed with 4% paraformaldehyde solution. The cells were stained with calcein-AM and PI, and observed with Olympus IX71 biological inverted microscope (JPN), according to the manufacturer's suggested protocol.

2.7. Animals and Tumor Model. Animals received care in accordance with the Guidance Suggestions for the Care and Use of Laboratory Animals.[16] The procedures were approved by Shenzhen Institutes of Advanced Technology, Chinese Academy of Sciences Animal Care and Use Committee.[16] MCF-7 cells (1×10^6) were subcutaneously injected into the flank region of the 4–6 weeks old female BALB/c nude mice (Vital River Laboratory Animal Technology Co. Ltd, CHN). Tumor volume was calculated as (tumor length) × (tumor width)^2/2.[16]

2.8. *in Vivo* Imaging and Biodistribution Analysis. Mice bearing MCF-7 tumors were randomly assigned into two groups, when the tumor volumes grew up to 100-200 mm^3. Mice were injected via tail vein with 200 μL free ICG or FA-INPs (both containing 176 μg/mL ICG). The CRi maestro ex *in vivo* imaging system (USA) was used to obtain the fluorescence signals of ICG (704 nm excitation and 735 nm filter) at 0.5, 6, 24, 48, and 72 h after injection. The mice were killed at 48 h after injection. The heart, liver, spleen, lung, kidneys, and tumor were collected for imaging and semiquatitative biodistribution analysis.

2.9. Temperature Measurements during Laser Irradiation. Centrifuge tubes was added PBS (0.5 mL), free ICG (0.5 mL, containing 65 μg/mL ICG) or FA-INPs (0.5 mL, containing 65 μg/mL ICG). Free ICG or FA-INPs (both containing 176 μg/mL ICG) was injected into the nude mice bearing MCF-7 tumor via tail vein. Control mice were injected with 200 μL PBS. The 808-nm laser at 1 W/cm^2 irradiated the tubes and tumors (at 48 h after intravenous injection) for 5 min. Fluke Ti27 infrared thermal imaging camera (USA) obtained infrared thermographic maps and region maximum temperatures. The photothermal conversion efficiency (η) of the FA-INPs or free ICG was calculated using the following equation:[27]

$$\eta = \frac{m_D C_D}{\tau_S} \times \frac{T_{max} - T_{surr} - Q_{Dis}}{I(1 - 10^{-A})}$$

where m_D (or C_D) is the mass (or heat capacity) of water, and τ_S is the system time constant of the sample, respectively.[27] Q_{Dis} expresses the heat dissipation from the light absorbed by the quartz sample cell, T_{max} (or T_{Surr}) is the equilibrium

temperature (or ambient temperature), I is the incident laser power (I = 1 W/cm^2), and A is the sample absorbance at 808 nm.[27] To detect the effect of photothermal therapy *in vivo*, hematoxylin and eosin stained the major organs on 15 d and tumors at 12 h after treatment.

The mice (5 per group) were intravenously injected with 200 μL PBS, free ICG (containing 176 μg/mL ICG), FA-INPs (containing 176 μg/mL ICG). For the laser treatment groups, the 808-nm laser irradiated the tumors of mice after 48 h at 1 W/cm^2 post-injection for 5 min. The tumor volumes and body weight of mice were recorded.

2.10. Statistical Analysis. All data are reported as mean ± standard error of the mean. One-way ANOVA analysis, followed by Tukey's post test, determined the differences among groups. Here, a single asterisk (*) indicated $P < 0.05$, and a double asterisk (**) indicated $P < 0.01$.[19]

3. RESULTS AND DISCUSSION

The FA-INPs were fabricated with ICG, lecithin, and DSPE-PEG-FA through film hydration via strong sonication followed by extrusion technique. Specifically, lecithin and DSPE-PEG-FA via self-assembly structured a lipid bilayer covered by FA targeted group, and the ICG was encapsulated in the particles. The results of transmission electron microscopy (TEM) demonstrated that the FA-INPs were ultrasmall with good monodispersity and ~90% FA-INPs in number distribution were 20−40 nm (see Figures 1A and 1B). The EE of ICG loaded in NPs was 43.75%. A size stability assay of the FA-INPs was performed under four different conditions: ultrapure water, PBS, 10% (V/V) plasma/heparin in PBS, and fetal bovine serum for 5 days at 37 °C (Figure 1E).[28] The long-term stability of NPs was investigated by placing the FA-INPs in PBS. The particle size of the FA-INPs in the PBS and ultrapure water remained the similar size (about 31 nm), suggesting a great long-term stability of the FA-INPs. And stability for protein binding was tested by putting the FA-INPs in plasma/heparin solution or serum.[28] The size of the NPs increased ~15 nm and the FA-INPs kept the size for 5 days, indicating protein binding of plasma was not an important factor. The FA-INPs maintained excellent stability without exhibiting any precipitation and phase separation in ultrapure water, PBS, plasma/heparin solution, and serum.

Compared with free ICG, the apsorption spectra and fluorescence spectra of the FA-INPs were demonstrated (Figures 1C, 1D). The absorption peak or emission peak of the FA-INPs was found to be red-shifted 10 nm (to 787 nm) or 1 nm (to 810 nm), respectively (Figures 1C, 1D). After 1 day, the ICG fluorescence intensity of the FA-INPs in ultrapure water remained at ~90%, while the ICG fluorescence intensity of free ICG in ultrapure water degraded to 65.24% (Figure 1F). Figure 1F also showed that the fluorescence intensity of free ICG in ultrapure water was decreased to 25.28% of initially intensity within 4 days, but the ICG fluorescence intensity of the FA-INPs in ultrapure water remained above 72%. NPs encapsulation significantly enhanced the fluorescence stability of ICG. We also measured the fluorescence intensity of the FA-INPs in PBS and serum for 4 days, the FA-INPs had no obvious change in any mediums of the ultrapure water, PBS and serum. Φ_F for the FA-INPs or free ICG in aqueous solution was 7.5% or 3.9% on day 0, and 4.89% or 0.97% on day 4. It suggested that the FA-INPs formulation strongly enhanced the ICG fluorescence properties, and the data were consistent with the reported optical properties assay.[26]

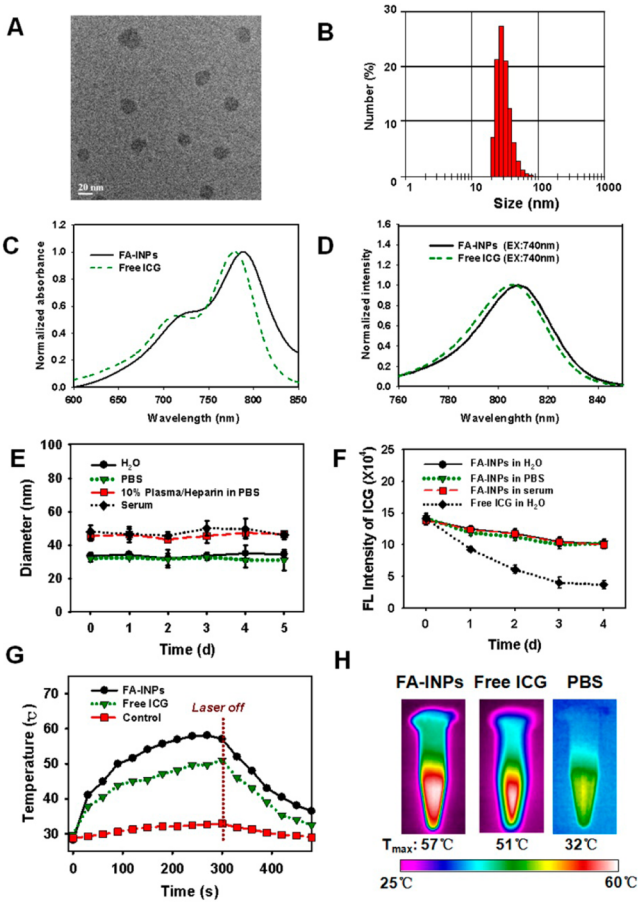

Figure 1. Characterization of the FA-INPs: (A) TEM image of the FA-INPs; (B) particle number distribution of the FA-INPs; (C) absorption spectra of the FA-INPs and free ICG (the absorption peak of the FA-INPs was red-shifted 10 nm to 787 nm); (D) fluorescence spectra of the FA-INPs and free ICG (the emission peak of the FA-INPs was only red-shifted 1 nm to 810 nm); (E) size stability of the FA-INPs (the FA-INPs maintained excellent stability without exhibiting any precipitation and phase separation in ultrapure water, PBS, 10% (V/V) plasma/heparin in PBS and serum); (F) ICG fluorescence stability of the FA-INPs (the fluorescence stability of ICG was significantly improved by the encapsulation of NPs, and the fluorescence of the FA-INPs showed no apparent change in any mediums of the ultrapure water, PBS, and serum); (G) photothermal effect of the FA-INPs, free ICG, and PBS as a function of the irradiation time under continuous 808-nm laser irradiation at a power intensity of 1 W/cm^2 (the irradiation lasted for 5 min, and then the laser was shut off); and (H) infrared thermographic maps of centrifuge tubes with the FA-INPs, free ICG, or PBS were measured at 5 min.

An infrared thermal imaging camera was used to measure the photothermal efficiency of the FA-INPs under laser irradiation. The maximum temperature (T_{max}) of the FA-INPs or free ICG reached 57 or 51 °C with the 1 W/cm^2 laser irradiation for 5 min, but the PBS with the same laser irradiation only increased to 32 °C (Figures 1G, 1H). The temperature increase of the FA-INPs was enough to irreversibly destroy tumor cells.[23−31] The heat conversion efficiency of the FA-INPs was calculated to be 17.3%, and it is higher than the heat conversion efficiency (15.1%) of the free ICG. The encapsulation of ICG in the NPs enhanced the heat conversion efficiency of free ICG.

The MCF-7 cellular uptake of the FA-INPs was tested *in vitro* (Figure 2A). After 2 h of incubation, the FA-INPs treated cells presented significantly higher fluorescence intensity in the

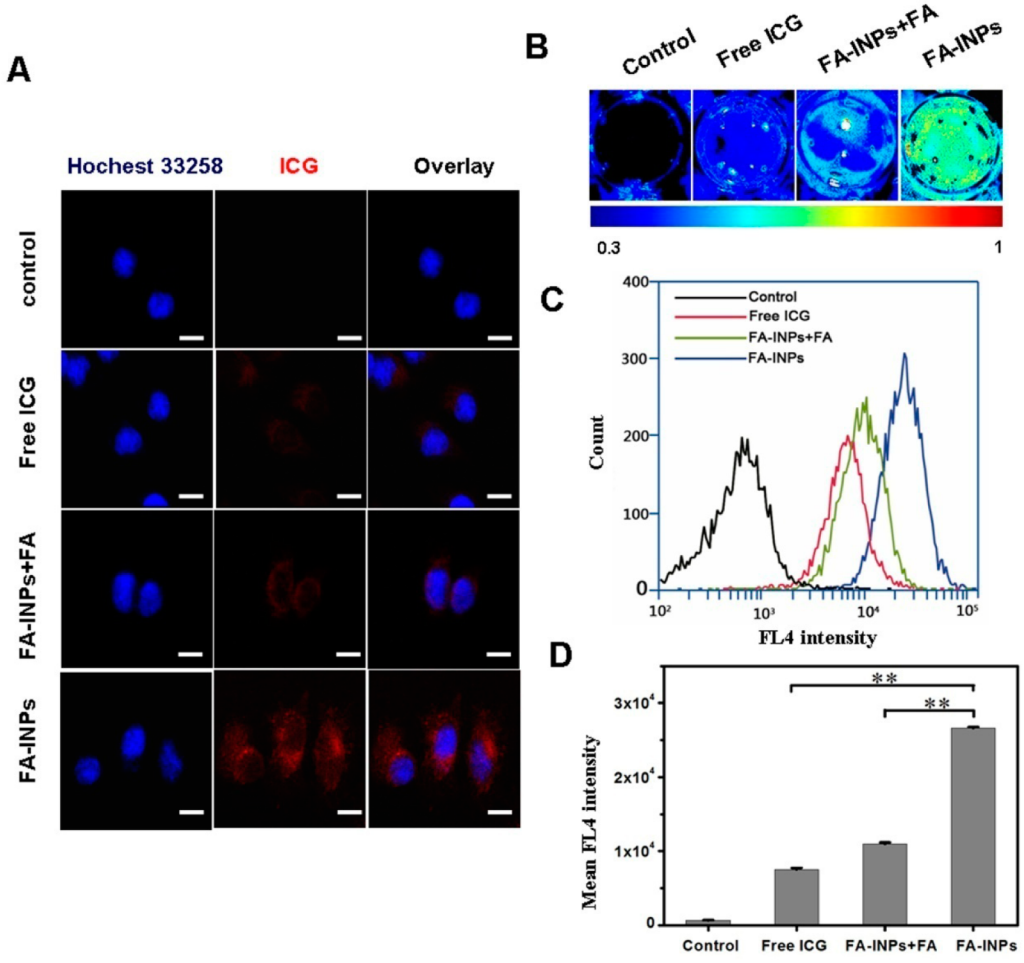

Figure 2. Endocytosis of the FA-INPs by MCF-7 cells after 2 h incubation: (A) MCF-7 confocal images of free ICG, FA-INPs, or FA-INPs + FA (blue represents the fluorescence of Hoechest 33258, and red represents the fluorescence of ICG; scale bar = 15 μm); (B) the NIR images of culture plates with MCF-7 cells after incubation with free ICG, FA-INPs, or FA-INPs + FA; (C) histograms for flow cytometry of MCF-7 cells after incubation with free ICG, FA-INPs, or FA-INPs + FA; and (D) mean fluorescence intensity analysis for flow cytometry of MCF-7 cells after incubation with free ICG, FA-INPs, or FA-INPs + FA.

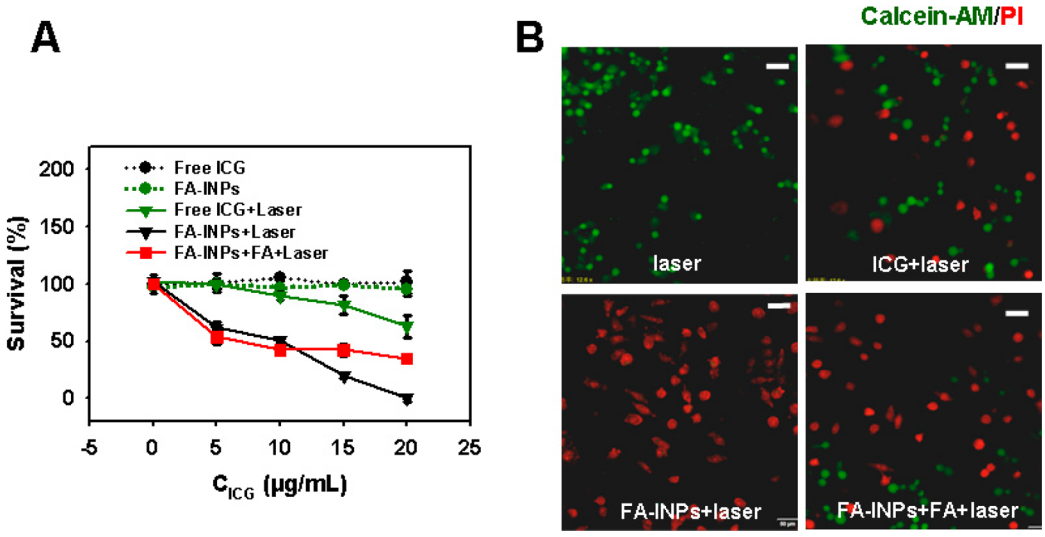

Figure 3. The photothermal effect on MCF-7 cells under different treatments: (A) survival of MCF-7 cells versus ICG concentration in free ICG, FA-INPs, free ICG + laser, FA-INPs + laser or FA-INPs + FA + laser treatments, and (B) fluorescence images of MCF-7 cells with the treatments of laser, ICG + laser, FA-INPs + laser, or FA-INPs + FA + laser. The ICG concentration was kept the same as 20 μg/mL. Viable cells were stained green with calcein-AM, and dead cells were stained red with PI. (Scale bar = 35 μm.)

dx.doi.org/10.1021/am5004393 | ACS Appl. Mater. Interfaces 2014, 6, 6709−6716

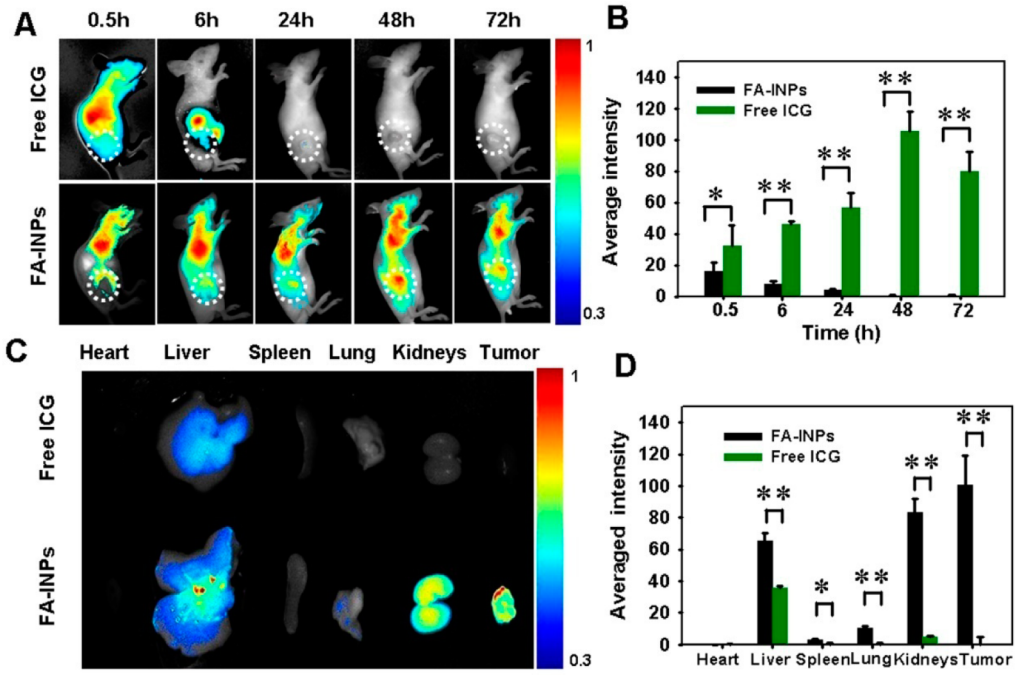

Figure 4. *In vivo* imaging and biodistribution analysis of nude mice bearing MCF-7 tumors after tail vein injected of free ICG and FA-INPs: (A) time-lapse NIR fluorescence images of nude mice (the tumors are circled with a dotted line); (B) NIR fluoresence intensities of the tumors were quantified at indicated time points; (C) NIR fluorescence images of major organs and tumors after 48 h post-injection of free ICG and FA-INPs; and (D) semiquantitative biodistribution of free ICG and FA-INPs in nude mice determined by the averaged fluorescence intensity of each organ. The data are shown as mean ± SD (n = 3); a single asterisk (*) indicates $P < 0.05$, and a double asterisk (**) indicates $P < 0.01$.

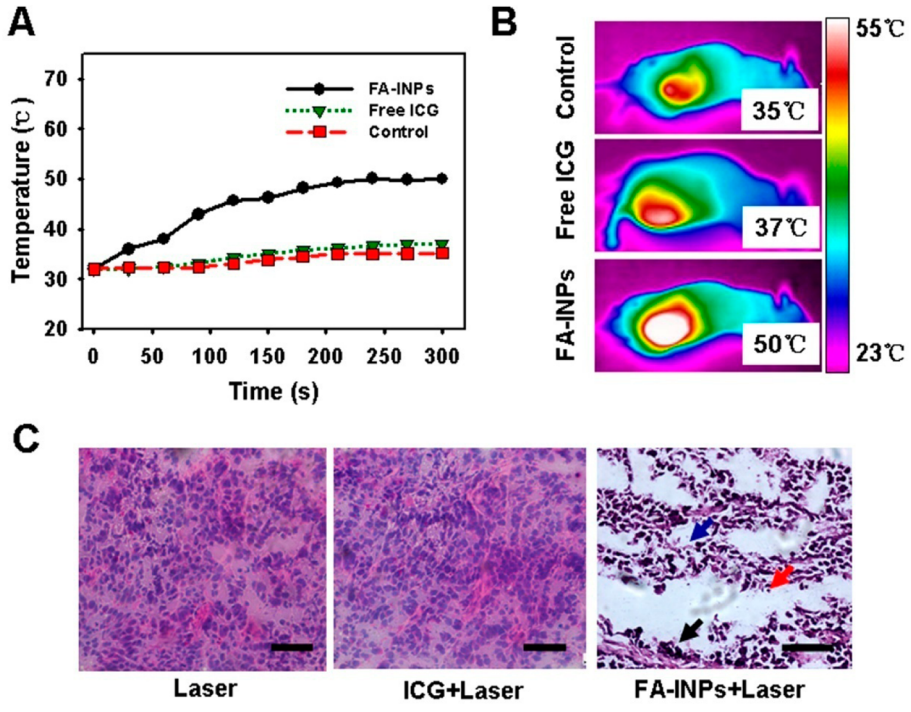

Figure 5. Photothermal therapy of nude mice bearing MCF-7 tumors (at 48 h after intravenous injection) following 1 W/cm^2 NIR laser irradiation: (A) maximum temperature profile of the irradiated area, as a function of the irradiation time; (B) infrared thermographic map of mice bearing MCF-7 tumors under different treatments was measured at 5 min with a thermal camera after NIR irradiation; (C) histological staining of the excised tumors 12 h after different treatments. Features of thermal damage were identified in tumors treated with the FA-INPs, such as coagulative necrosis (black arrow), abundant pykonosis (blue arrow), and considerable regions of karyolysis (red arrow). (Scale bar = 50 μm.)

cytoplasm, indicating the endocytosis of the FA-INPs was stronger than that of free ICG. With the competition-blocking of free FA, the fluorescence intensity of the FA-INPs + FA treatment in the cytoplasm decreased, but the fluorescence intensity was stronger than that of free ICG. Such results were further demonstrated by the NIR images obtained by the ex *in*

dx.doi.org/10.1021/am5004393 | ACS Appl. Mater. Interfaces 2014, 6, 6709−6716

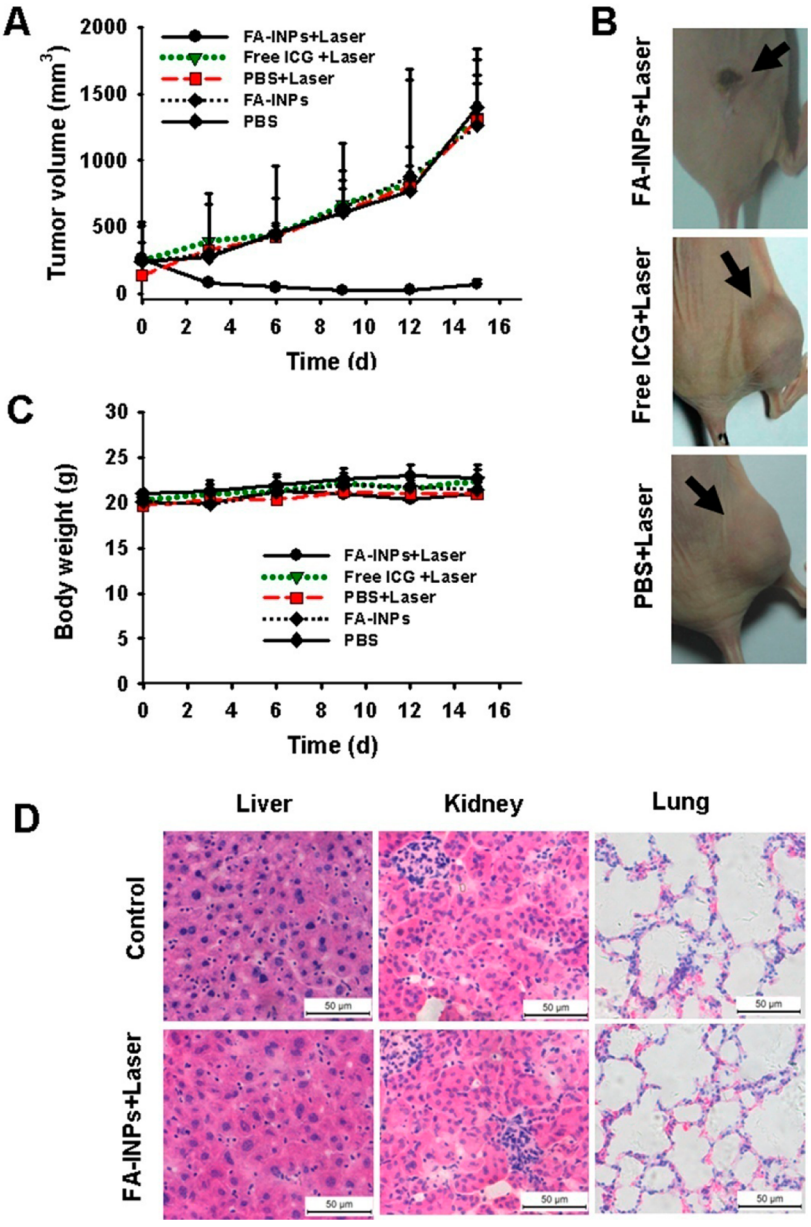

Figure 6. *In vivo* photothermal therapy of the FA-INPs: (A) MCF-7 tumor growth curves of different groups after treatments; (B) representative photos of mice on 15 d after various treatment (the tumors were marked by the blank arrows); (C) body weight of mice in different groups after treatment; and (D) H&E stained images of the liver, kidneys, and lungs from untreated healthy mice and treated mice with FA-INPs injection taken 15 days after photothermal therapy. No noticeable abnormality was observed in major organs including liver, kidneys, and lungs. (Scale bar = 50 μm.)

vivo imaging system and flow cytometry analysis (Figures 2B, 2C, 2D). These results revealed consistently that the FA-INPs significantly increased the endocytosis ability of ICG (Figures 2B, 2C, 2D). Conjoint incubation with the FA-INPs and 200 μg/mL of free FA yielded a lower level of cellular uptake as compared to the FA-INPs, but showed stronger fluorescence intensity than incubation with free ICG (Figures 2B, 2C, 2D). These proved that NPs formulation improved internalization of ICG. In the meantime, FA active-targeting mediated endocytosis of the FA-INPs further significantly enhanced the cellular uptake of the NPs.

We studied the *in vitro* photothermal toxicity of FA-NPs in MCF-7 cells. With laser irradiation, incubation with free ICG (containing 20 μg/mL of ICG) caused the death of ~36% of cells (Figure 3A). The FA-INPs + laser group with 20 μg/mL of ICG induced the death of up to 100% of cells, suggesting that FA-INPs could effectively target FA over-expressing MCF-7 cells and enhanced ICG concentration in MCF-7 cells (Figure 3A). With the competition-blocking of free FA, the endocytosis of MCF-7 cells treated by FA-INPs + FA + laser was prohibited and viability of cells significantly decreased to 34.83% (Figure 3A). Figure 3A also showed that no toxic effect was exhibited in the MCF-7 cells treated with free ICG or FA-INPs (containing 20 μg/mL of ICG), indicating that the free ICG or FA-INPs were biocompatible at this concentration. The fluorescence staining of live/dead cells was agreed well with the MTT assay (Figure 3B).

We measured the amounts of the FA-INPs accumulated in tumor and organs using the sensitive and intrinsic NIR fluorescence of ICG. Figure 4A showed that the fluorescence

dx.doi.org/10.1021/am5004393 | ACS Appl. Mater. Interfaces 2014, 6, 6709−6716

signals of free ICG group at 0.5 h after injection were whole body distribution and mainly located in the liver. Fluorescence signals of the free ICG group at 6 h were almost located around the intestine, and no obvious signals were detected at 24, 48, or 72 h in Figure 4A. However, the FA-INPs showed a different biodistribution behavior. The ICG fluorescence intensity of the whole nude mice at 72 h post-injection for FA-NPs still retained strong fluorescence signals. These data further confirmed that FA-INPs encapsulation could significantly reduce clearance from the body and degradation of ICG. In the meantime, the FA-INPs located in the liver and around the tumor at 0.5 h, and fluorescence signals in the tumor at 6, 24, and 48 h, were progressively strengthened. However, the fluorescence intensity in the tumor reduced after 72 h post-injection of the FA-INPs. According to the dynamic NIR fluorescence of ICG, 48 h after post-injection were chosen as the time point of photothermal therapy in order to obtain the maximum efficacy.

The tumors and major organs distribution of free ICG and FA-INPs after 48 h post-injection are also shown in Figures 4C, 4D. After injection of free ICG, most of the ICG gathered in the liver at 48 h. The FA-INPs obviously promoted the accumulation of ICG in tumor, followed by kidneys, liver, lung and spleen. The fluorescence analysis showed that the averaged intensity in tumor of the FA-INPs formulation was 200 times higher than that of free ICG. It was worth mentioning that the limit of penetration depths of ICG fluorescence leaded that no fluorescence signals at 48 h *in vivo* were seen for the free ICG group, but there were detectable fluorescence signals in the excised liver at 48 h.

We measured the intratumoral temperature while the nude mice at 48 h after intravenous injection with PBS, free ICG, and FA-INPs was irradiated for 5 min with a NIR laser. Because of the EPR of NPs in tumor and specific accumulation of the FA-INPs in tumor, the tumors treated with the FA-INPs had a maximum temperature of 50 °C (Figures 5A, 5B) after the 5 min of laser irradiation, which exceeded the destroy threshold needed to cause irreversible tumor damage.[20,31] Typical thermal damage characteristics of the tumors were showed in the FA-INPs plus laser treatmemt, such as necrosis, pykonosis, and karyolysis (Figure 5C). Tumors treated with PBS plus laser or free ICG plus laser for 5 min generated the maximum temperature of 35 °C or 37 °C (Figures 5A, 5B), those were not enough to irreversibly destroy tumors.[32−34] The PBS or free ICG group had no apparent influence on the tumors (Figure 5C).

We examined the anti-cancer effect of FA-INPs plus laser in MCF-7 tumor-bearing nude mice. The MCF-7 tumors treated with PBS or PBS under laser irradiation showed rapid growth, suggesting that the laser irradiation did not affected the tumor growth (Figure 6A). The FA-INPs without laser or free ICG plus laser group had no apparent influence on tumors (Figure 6A). Because of the specific accumulation of the FA-INPs in tumors and EPR of NPs in tumors, FA-INPs under laser irradiation caused a complete tumor ablation, leaving a black scar in the original tumor site after 15 d (Figures 6A, 6B). Body weight did not significantly change in either treatment (Figure 6C). The FA-INPs significantly increased the accumulation of the ICG in kidneys, liver, and lung, so we further investigated the potential toxicity of the FA-INPs and laser irradiation in the kidneys, liver, and lungs. H&E staining of the liver, kidneys, and lungs showed no noticeable organ damage 15 d after photothermal therapy of the FA-INPs (Figure 6D). Therefore, the results suggested that FA-INPs did not cause evident side effects to the normal tissue and organs.

4. CONCLUSIONS

The well-defined FA-INPs were successfully prepared, using the film hydration via strong sonication followed by extrusion technique for small FA targeting NPs. The FA-INPs remarkably enhanced ICG stability, produced stronger temperature response than free ICG under 808-nm laser irradiation, and exhibited significant targeting to MCF-7 cells and MCF-7 tumors. The NIR image-guided photothermal therapy of FA-INPs not only highly induced *in vitro* MCF-cell death, but also efficiently inhibited the growth of the MCF-7 tumor *in vivo*. Moreover, histological examination shows no evident side effect of the FA-INPs to mice within 15 days. These results clearly prove that the FA-INPs are notable theranostic agents for imaging-guided cancer therapy and have great potential in clinical applications.

AUTHOR INFORMATION

Corresponding Author

*Tel: +86-755-86392210. E-mail: lt.cai@siat.ac.cn.

Author Contributions

§These authors contributed equally to this work.

Notes

The authors declare no competing financial interest.

ACKNOWLEDGMENTS

The authors gratefully acknowledge support for the National Natural Science Foundation of China (Grant Nos. 81071249, 81171446, and 20905050), Guangdong Innovation Team of Low-Cost Healthcare, Science and Technology Key Project of Guangdong (No. 2009A030301010), Shenzhen (Nos. CXB201005250029A, JC201005270326A, JC201104220242A, JC201005260247A), and Cultivation Fund of Guangdong Medical College (No. XK1426).

REFERENCES

(1) Siegel, R.; Naishadham, D.; Jemal, A. Cancer statistics, 2012. *Ca—Cancer J. Clin.* **2012**, *62*, 10−29.

(2) Shanbhag, P. P.; Jog, S. V.; Chogale, M. M.; Gaikwad, S. S. Theranostics for Cancer Therapy. *Curr. Drug Delivery* **2013**, *10*, 357−362.

(3) Brigger, I.; Dubernet, C.; Couvreur, P. Nanoparticles in Cancer Therapy and Diagnosis. *Adv. Drug Delivery Rev.* **2012**, *64*, 24−36.

(4) Davis, M. E. Nanoparticle therapeutics: An emerging treatment modality for cancer. *Nat. Rev. Drug Discovery* **2008**, *7*, 771−782.

(5) Bardhan, R.; Lal, S.; Joshi, A.; Halas, N. J. Theranostic Nanoshells: From Probe Design to Imaging and Treatment of Cancer. *Acc. Chem. Res.* **2011**, *44*, 936−946.

(6) Luk, B. T.; Fang, R. H.; Zhang, L. Lipid-and Polymer-based Nanostructures for Cancer Theranostics. *Theranostics* **2012**, *2*, 1117−1126.

(7) Morgan, B. Opportunities and Pitfalls of Cancer Imaging in Clinical Trials. *Nat. Rev. Clin. Oncol.* **2011**, *8*, 517−527.

(8) Zheng, M.; Gong, P.; Jia, D.; Zheng, C.; Ma, Y.; Cai, L. PLGA−Lecithin−PEG Core−shell Nanoparticles for Cancer Targeted Therapy. *Nano LIFE* **2012**, *2*, 125002.

(9) Park, K.; Lee, S.; Kang, E.; Kim, K.; Choi, K.; Kwon, I. C. New Generation of Multifunctional Nanoparticles for Cancer Imaging and Therapy. *Adv. Funct. Mater.* **2009**, *19*, 1553−1566.

(10) Smith, A. M.; Nie, S. Next-generation Quantum Dots. *Nat. Biotechnol.* **2009**, *27*, 732−733.

(11) Veiseh, O.; Gunn, J. W.; Zhang, M. Design and Fabrication of Magnetic Nanoparticles for Targeted Drug Delivery and Imaging. *Adv. Drug Delivery Rev.* **2010**, *62*, 284−304.
(12) Kim, D.; Jeong, Y. Y.; Jon, S. A Drug-loaded Aptamer−Gold Nanoparticle Bioconjugate for Combined CT Imaging and Therapy of Prostate Cancer. *ACS Nano* **2010**, *4*, 3689−3696.
(13) Xia, Y.; Li, W.; Cobley, C. M.; Chen, J.; Xia, X.; Zhang, Q.; Yang, M.; Cho, E. C.; Brown, P. K. Gold Nanocages: from Synthesis to Theranostic Applications. *Acc. Chem. Res.* **2011**, *44*, 914−924.
(14) Santra, S.; Kaittanis, C.; Grimm, J.; Perez, J. M. Drug/Dye-Loaded, Multifunctional Iron Oxide Nanoparticles for Combined Targeted Cancer Therapy and Dual Optical/Magnetic Resonance Imaging. *Small* **2009**, *5*, 1862−1868.
(15) Nie, L.; Wang, S.; Wang, X.; Rong, P.; Ma, Y.; Liu, G.; Huang, P.; Lu, G.; Chen, X. *In vivo* Volumetric Photoacoustic Molecular Angiography and Therapeutic Monitoring with Targeted Plasmonic Nanostars. *Small* **2013**, *8*, 385−391.
(16) Zheng, C.; Zheng, M.; Gong, P.; Jia, D.; Zhang, P.; Shi, B.; Sheng, Z.; Ma, Y.; Cai, L. Indocyanine Green-loaded Biodegradable Tumor Targeting Nanoprobes for *In Vitro* and *In Vivo* Imaging. *Biomaterials* **2012**, *33*, 5603−5609.
(17) Li, J.; Jiang, H.; Yu, Z.; Xia, H.; Zou, G.; Zhang, Q.; Yu, Y. Multifunctional Uniform Core−Shell Fe_3O_4@ $mSiO_2$ Mesoporous Nanoparticles for Bimodal Imaging and Photothermal Therapy. *Chem.−Asian J.* **2013**, *8*, 385−391.
(18) Zheng, X.; Zhou, F.; Wu, B.; Chen, W. R.; Xing, D. Enhanced Tumor Treatment using Biofunctional Indocyanine Green-containing Nanostructure by Intratumoral or Intravenous Injection. *Mol. Pharm.* **2012**, *9*, 514−522.
(19) Zheng, M.; Yue, C.; Ma, Y.; Gong, P.; Zhao, P.; Zheng, C.; Sheng, Z.; Zhang, P.; Wang, Z.; Cai, L. Single-Step Assembly of DOX/ICG Loaded Lipid−Polymer Nanoparticles for Highly Effective Chemo-photothermal Combination Therapy. *ACS Nano* **2013**, *7*, 2056−2067.
(20) Nomikou, N.; Sterrett, C.; Arthur, C.; McCaughan, B.; Callan, J. F.; McHale, A. P. The Effects of Ultrasound and Light on Indocyanin-Green-Treated Tumour Cells and Tissues. *ChemMedChem.* **2012**, *7*, 1465−1471.
(21) Yaseen, M. A.; Yu, J.; Wong, M. S.; Anvari, B. Laser-Induced Heating of Dextran-Coated Mesocapsules Containing Indocyanine Green. *Biotechnol. Prog.* **2007**, *23*, 1431−1440.
(22) Kirchherr, A.-K.; Briel, A.; Mader, K. Stabilization of Indocyanine Green by Encapsulation within Micellar Systems. *Mol. Pharm.* **2009**, *6*, 480−491.
(23) Al-Jamal, W. T.; Al-Jamal, K. T.; Cakebread, A.; Halket, J. M.; Kostarelos, K. Blood Circulation and Tissue Biodistribution of Lipid−Quantum Dot (L-QD) Hybrid Vesicles Intravenously Administered in Mice. *Bioconjugate Chem.* **2009**, *20*, 1696−1702.
(24) Al-Ahmady, Z. S.; Al-Jamal, W. T.; Bossche, J. V.; Bui, T. T.; Drake, A. F.; Mason, A. J.; Kostarelos, K. Lipid−Peptide Vesicle Nanoscale Hybrids for Triggered Drug Release by Mild Hyperthermia *In Vitro* and *In Vivo*. *ACS Nano* **2012**, *6*, 9335−9346.
(25) Dicheva, B. M.; ten Hagen, T. L.; Li, L.; Schipper, D.; Seynhaeve, A. L.; van Rhoon, G. C.; Eggermont, A. M.; Lindner, L. H.; Koning, G. A. Cationic Thermosensitive Liposomes: A Novel Dual Targeted Heat-triggered Drug Delivery Approach for Endothelial and Tumor Cells. *Nano Lett.* **2013**, *13*, 2324−2331.
(26) Navarro, F. P.; Berger, M.; Goutayer, M.; Guillermet, S.; Josserand, V.; Rizo, P.; Vinet, F.; Texier, I. A Novel Indocyanine Green Nanoparticle Probe for non Invasive Fluorescence Imaging *In Vivo*. *Proc. SPIE* **2009**, *71900L*, 1−10.
(27) Tian, Q.; Jiang, F.; Zou, R.; Liu, Q.; Chen, Z.; Zhu, M.; Yang, S.; Wang, J.; Wang, J.; Hu, J. Hydrophilic Cu_9S_5 Nanocrystals: A Photothermal Agent with a 25.7% Heat Conversion Efficiency for Photothermal Ablation of Cancer Cells In Vivo. *ACS Nano* **2011**, *5*, 9761−9771.
(28) Chan, J. M.; Zhang, L.; Yuet, K. P.; Liao, G.; Rhee, J.-W.; Langer, R.; Farokhzad, O. C. PLGA−Lecithin−PEG Core−Shell Nanoparticles for Controlled Drug Delivery. *Biomaterials* **2009**, *30*, 1627−1634.
(29) Zheng, X.; Zhou, F.; Wu, B.; Chen, W. R.; Xing, D. Enhanced Tumor Treatment Using Biofunctional Indocyanine Green-Containing Nanostructure by Intratumoral or Intravenous Injection. *Mol. Pharm.* **2012**, *9*, 514−522.
(30) Yue, C.; Liu, P.; Zheng, M.; Zhao, P.; Wang, Y.; Ma, Y.; Cai, L. IR-780 dye loaded Tumor Targeting Theranostic Nanoparticles for NIR Imaging and Photothermal Therapy. *Biomaterials* **2013**, *34*, 6853−6861.
(31) Lim, Y. T.; Noh, Y. W.; Han, J. H.; Cai, Q. Y.; Yoon, K. H.; Chung, B. H. Biocompatible Polymer−Nanoparticle-Based Bimodal Imaging Contrast Agents for the Labeling and Tracking of Dendritic Cells. *Small* **2008**, *4*, 1640−1645.
(32) Hirsch, L. R.; Stafford, R.; Bankson, J.; Sershen, S.; Rivera, B.; Price, R.; Hazle, J.; Halas, N.; West, J. Nanoshell-mediated Near-infrared Thermal Therapy of Tumors under Magnetic Resonance Guidance. *Proc. Natl. Acad. Sci. U.S.A.* **2003**, *100*, 13549−13554.
(33) Tang, Y.; McGoron, A. J. Combined Effects of Laser-ICG Photothermotherapy and Doxorubicin Chemotherapy on Ovarian Cancer Cells. *J. Photochem. Photobiol., B* **2009**, *97*, 138−144.
(34) Zhang, J.; Jin, W.; Wang, X.; Wang, J.; Zhang, X.; Zhang, Q. A novel Octreotide Modified Lipid Vesicle improved the Anticancer Efficacy of Doxorubicin in Somatostatin Receptor 2 Positive Tumor Models. *Mol. Pharm.* **2010**, *7*, 1159−1168.